Available online at www.sciencedirect.com
ScienceDirect
Journal of Computational Physics 226 (2007) 2372–2388
JOURNAL OF COMPUTATIONAL PHYSICS
www.elsevier.com/locate/jcp

Optimized three-dimensional FDTD discretizations of Maxwell's equations on Cartesian grids

Theodoros T. Zygiridis, Theodoros D. Tsiboukis *

Applied and Computational Electromagnetics Laboratory, Department of Electrical and Computer Engineering, Aristotle University of Thessaloniki, Thessaloniki 54124, Greece

Received 6 February 2007; received in revised form 16 July 2007; accepted 17 July 2007
Available online 27 July 2007

Abstract

In this paper, novel finite-difference time-domain (FDTD) schemes are introduced for the numerical solution of Maxwell's equations on dual staggered Cartesian three-dimensional lattices. The proposed techniques are designed to accomplish optimized performance according to certain features and requirements dictated by the investigated problems, thus making efficient use of the available computational resources. Starting from only few initial assumptions, a construction process based on the minimization of specific error formulae is developed, which is later exploited to derive the final form of the finite-difference operators. Previously, an elaborate analysis of the proposed indicators is provided, targeting at global error control over all propagation angles. Our methodology guarantees upgraded flexibility, as accuracy can be maximized within either narrow or wider frequency bands, without practically inducing significant computational overhead. Attractive qualities such as high convergence rates are now the natural consequence of the effective design process, rather than the minimization of the truncation errors of the difference expressions. In fact, the proposed FDTD approaches verify the possibility to attain improved levels of accuracy, without resorting to the traditional – Taylor based – forms of the individual operators. A theoretical analysis of the inherent dispersion artifacts reveals the full potential of the new algorithms, while numerical tests and comparisons unveil their unquestionable merits in practical applications.

Keywords: Finite differences; Time-domain methods; Higher-order schemes; Numerical dispersion; Optimization

1. Introduction

The continuous scientific research in the computational electromagnetics area, stimulated and motivated by various engineering applications, has led to the development of diverse numerical techniques for the simulation of wave-interaction phenomena. Among them, the finite-difference time-domain (FDTD) method has been established as a relatively simple, efficient and adequately accurate – in several instances – numerical tool [1,2]. Through extensive testing during the previous years, the FDTD algorithm has been proven to be

* Corresponding author. Tel.: +30 2310 996323; fax: +30 2310 996312.
E-mail address: tsibukis@auth.gr (T.D. Tsiboukis).

0021-9991/$ - see front matter
doi:10.1016/j.jcp.2007.07.008

especially suited for problems incorporating domains of small or moderate at most electrical size. Unfortunately, its accuracy is rendered questionable when studying electrically large structures. Moreover, poor performance may be observed even in small-scale simulations, if stringent accuracy requirements must be fulfilled for elongated time periods. Such undesirable situations are the natural consequences of the adopted second-order space–time approximations, and can undoubtedly constitute limiting factors when investigating electromagnetic problems of contemporary interest.

In essence, the FDTD-related inaccuracies do not manifest themselves as randomly distributed or generated errors, but appear with the form of numerical dispersion and anisotropy artifacts. The latter are recognized as one of the most significant sources of error (others may be related to the rather limited geometric flexibility of the structured Cartesian grids), whose detrimental consequences are further aggravated by their accumulative nature. As a result, fundamental properties of electromagnetic waves may not be always preserved to a reliable degree in simulations entailing energy propagation, thereby producing misleading numerical conclusions.

Unfortunately, within the rather limited framework of Yee's algorithm, the available choices for accuracy upgrade are directly related to the adoption of finer grid resolutions (which, due to stability limitations, also imply smaller time-steps). This kind of solutions is rarely attractive, as the low order of the classic FDTD method renders mesh refining quite costly (and often prohibitive). On the other hand, notable accuracy improvement can be ensured if the second-order approximations are replaced by higher-order counterparts, which are capable of accomplishing reduced error levels under the same computational cost. The relevant bibliography comprises various FDTD techniques that adopt high-order alternatives, such as explicit [3,4] or implicit [5–7] spatial approximations, combined with enhanced time-integration processes, including leapfrog and Runge–Kutta schemes [8], backward approximations [9], symplectic integrators [10], etc.

Since the best compromise between accuracy and computational cost remains an open matter for FDTD methodologies, the fundamental question that needs to be answered is concerned with the characterization of the adequacy or suitability of a finite-difference scheme for a given electromagnetic problem. In plain words, how the approximations to space–time derivatives should be designed (given e.g. the stencil size), in order to guarantee a solution with the highest degree of accuracy. On the other hand, it is generally recognized that maximizing the formal order in finite-difference expressions is not the optimum way to treat numerical simulations. Such an allegation simply implies that problems with different characteristics or accuracy requirements must not be dealt with in a unified manner. In accordance with this practice, there have been reported some instances – not only in computational electromagnetics – toward the design of problem-optimized finite differences. For example, modified compact schemes were derived in [11] by requiring the vanishing of an error formula at preselected frequency points, aiming for improvement at small wavelengths. Similarly, new approximate expressions were obtained in [12] through the solution of properly defined minimization problems, while control of both phase and amplitude errors was performed in [13]. Minimization of dispersion errors was also carried out in [14], where a $(2,4)$-like FDTD technique with high phase accuracy was developed, to deal with electrically large structures. A collection of finite-difference approaches that are capable of providing "flexible local approximations" was recently demonstrated in [15], referring to a wide variety of problems. As shown, these discretization strategies exploit the fact that specific features of the exact solutions are known a priori (the non-standard FDTD method [16,17], based on a single-frequency tuning, can be included in this category as well). Other higher-order FDTD algorithms [18,19] were optimized within specific frequency bands and/or angular sectors, based on the minimization of special error functionals. Modified schemes based on the $(2,4)$ stencil were constructed in [20], by minimizing errors along selected angles of propagation. A more generalized design methodology was presented in [21], which enabled the development of various algorithms through systematic modifications of their characteristic equations. We could also refer to some approaches that improve conventional FDTD methods by altering the constitutive parameters of the background media [22,23]. Apparently, they too can be considered equivalent to applying modified operators in conjunction with the physical materials.

It becomes clear that contemporary computational challenges dictate the establishment of a general design framework, founded on a solid theoretical basis, to enable flawless capturing and reproduction of electromagnetic properties in discrete spaces, without at the same time sacrificing the inherent simplicity of traditional FDTD methodologies. Towards this perspective, the present paper discusses the development of novel three-dimensional (3D) FDTD schemes with optimum discretization properties, suitable for solving demand-

ing electromagnetic problems with reasonable computational cost. Regarding their spectral accuracy, the proposed algorithms exhibit attractive as well as adaptive capabilities in frequency bands determined by the investigated problems. Contrary to conventional trends, their formulation avoids the preservation of maximum order of accuracy. Instead, estimation of the dispersion errors is pursued, according to formulae derived from the discrete Maxwell's equations, and the – initially parametric – finite-difference operators are then specified, by requiring the elimination of numerical inaccuracies. It is proved that optimization at a single-frequency point leads to techniques especially suited for time-harmonic problems, while the more challenging issue of wideband optimization is treated efficiently by performing error control at two distinct frequencies. A key feature of the new schemes is the geometric structure of the spatial approximations, which introduce additional sample points and posses a multidimensional configuration. Since the spectral reliability of the proposed approaches is directly associated to problem-related restrictions, efficient exploitation of computational resources is accomplished. The new algorithms thereby perform significantly better than traditional FDTD schemes, providing optimum discretization strategies for the electromagnetic equations on 3D computational grids. Their success is finally verified not only through theoretical investigation of the attained dispersion and anisotropy mitigation, but also by testing the proposed concepts in practical simulations.

2. Motivation for the development of novel FDTD schemes

The vast majority of the high-order FDTD methods proposed in the literature are based on difference operators that maximize the order of their truncation error, as the latter results from the implementation of Taylor series expansion. Specifically, symmetric expressions of the form

$$\left.\frac{\partial f}{\partial u}\right|_i = \frac{1}{\Delta u}\sum_{l=1}^{N/2} C_l\left(f|_{i+\frac{2l-1}{2}} - f|_{i-\frac{2l-1}{2}}\right) + \mathrm{O}(\Delta u^M) \tag{1}$$

are mainly selected for the spatial derivatives (asymmetrical stencils may introduce artificial dissipation, usually not required in the type of simulations considered here). Maximizing the formal order of the corresponding approximation simply implies that $M = N$. For instance, it is $C_1 = 1$ when $N = 2$, $C_1 = 9/8$ and $C_2 = -1/24$ when $N = 4$, and $C_1 = 75/64$, $C_2 = -25/384$ and $C_3 = 3/640$ when $N = 6$, defining operators of second, fourth and sixth order, respectively. Along similar lines, as shown in relevant publications, several time-integration schemes can be designed (including leapfrog, Runge–Kutta, or symplectic methods) by computing Taylor-based approximations of a matrix exponential, which corresponds to the exact solution of Maxwell's semi-discrete system.

As briefly mentioned in Section 1, our motivation for developing novel FDTD schemes is actually the fact that the traditional types of finite differences do not constitute optimum choices for dealing with numerical wave propagation. In essence, the utilization of Taylor-based approximations unavoidably stipulates the treatment of electromagnetic problems according to a unified practice. It is easily understood that special requirements pertinent to the examined problem are overlooked in this way. Let us not forget that the common origin of the aforementioned expressions has an obvious impact on algorithmic performance in the frequency domain. Since accuracy improves only when the discretization steps become smaller, low-frequency bands are always characterized by lower error levels. Apparently, this cannot be a sign of optimum performance. In other words, Taylor-based expressions lack the necessary flexibility to enable a problem-dependent manipulation. In addition, the shortcomings of conventional finite-differences also become obvious when spatial and temporal discretizations do not maintain identical formal orders. Consider for example, the case of the well-known (2,4) scheme [3,4]. The incorporation of the second-order time-stepping renders the fourth-order spatial approximations practically useless, unless very fine temporal increments are selected (a solution with high computational cost). In fact, we have shown in [24] alternative ways to significantly improve the accuracy of the (2,4) approach close to the stability limit, by sacrificing the formal accuracy and retaining the spatial stencil.

Consequently, we are motivated to construct FDTD techniques to deal with "difficult" electromagnetic problems, which may incorporate electrically extended domains (discretized with possibly coarse grids) and call for elongated time integration. As conventional formulations do not possess the necessary flexibility,

the proposed schemes are required to have certain properties, with the most significant one being the capability to adjust their reliability range in the frequency domain according to the examined problem's requirements. The fulfillment of this objective heavily relies on the following mathematical analysis, which aims at establishing a credible way of estimating discretization errors. In the next section, the foundation of the new FDTD methods is thoroughly explained.

3. Algorithmic structure and error estimators in 3D

3.1. General features

If we assume that electric and magnetic fields are staggered in time, then according to the standard leapfrog integrator the corresponding quantities can be approximated by the following update equations:[1]

$$\mathbf{H}|^{n+\frac{1}{2}}_{i_1,i_2,i_3} = \mathbf{H}|^{n-\frac{1}{2}}_{i_1,i_2,i_3} - \frac{\Delta t}{\mu}\tilde{\nabla}\times\mathbf{E}|^{n}_{i_1,i_2,i_3}, \tag{2}$$

$$\mathbf{E}|^{n+1}_{i_1,i_2,i_3} = \mathbf{E}|^{n}_{i_1,i_2,i_3} + \frac{\Delta t}{\epsilon}\tilde{\nabla}\times\mathbf{H}|^{n+\frac{1}{2}}_{i_1,i_2,i_3}, \tag{3}$$

where

$$\mathbf{E}|^{n}_{i_1,i_2,i_3} = \begin{bmatrix} E_x|^{n}_{i_1+\frac{1}{2},i_2,i_3} \\ E_y|^{n}_{i_1,i_2+\frac{1}{2},i_3} \\ E_z|^{n}_{i_1,i_2,i_3+\frac{1}{2}} \end{bmatrix}, \quad \mathbf{H}|^{n+\frac{1}{2}}_{i_1,i_2,i_3} = \begin{bmatrix} H_x|^{n+\frac{1}{2}}_{i_1,i_2+\frac{1}{2},i_3+\frac{1}{2}} \\ H_y|^{n+\frac{1}{2}}_{i_1+\frac{1}{2},i_2,i_3+\frac{1}{2}} \\ H_z|^{n+\frac{1}{2}}_{i_1+\frac{1}{2},i_2+\frac{1}{2},i_3} \end{bmatrix}. \tag{4}$$

The $\sim$ symbol over ∇ indicates that the exact nabla operator has been replaced by a discrete form. It should be mentioned that, although (2) and (3) resemble a formally second-order algorithm in time, higher-order leapfrog integrators possess a similar structure as well [8]. For the approximation of spatial derivatives, a parametric family of finite-difference expressions with various stencils is introduced. Specifically, the first derivative of a component f with respect to variable u, is calculated according to

$$\begin{aligned} \left.\frac{\partial f}{\partial u}\right|_{i_1,i_2,i_3} \simeq \frac{1}{\Delta u}\Bigg\{ & \sum_{l=1}^{N} C_l^u \left(f|_{i_1+\frac{2l-1}{2},i_2,i_3} - f|_{i_1-\frac{2l-1}{2},i_2,i_3} \right) \\ & + \sum_{l=1}^{M} D_l^v \left(f|_{i_1+\frac{2l-1}{2},i_2+1,i_3} + f|_{i_1+\frac{2l-1}{2},i_2-1,i_3} - f|_{i_1-\frac{2l-1}{2},i_2+1,i_3} - f|_{i_1-\frac{2l-1}{2},i_2-1,i_3} \right) \\ & + \sum_{l=1}^{M} D_l^w \left(f|_{i_1+\frac{2l-1}{2},i_2,i_3+1} + f|_{i_1+\frac{2l-1}{2},i_2,i_3-1} - f|_{i_1-\frac{2l-1}{2},i_2,i_3+1} - f|_{i_1-\frac{2l-1}{2},i_2,i_3-1} \right) \Bigg\} \end{aligned} \tag{5}$$

at position (u,v,w) (apparently, coordinate permutations yield rotated versions of (5) that correspond to $\frac{\partial}{\partial v}$ and $\frac{\partial}{\partial w}$ approximations). The stencil size and shape of the spatial operators is shown in Fig. 1, for various combinations of N, M. The numerical dispersion relation for this type of approximations is obtained by substituting appropriate Fourier modes in the discretized Maxwell's equations, and has the following form:

$$\begin{aligned} \frac{\sin^2\left(\frac{\omega\Delta t}{2}\right)}{c_0^2\Delta t^2} = \sum_{(u,v,w)} \frac{1}{\Delta u^2} \Bigg[& \sum_{l=1}^{N} C_l^u \sin\left(\frac{2l-1}{2}\tilde{k}_u\Delta u\right) \\ & + \sum_{l=1}^{M} 2\left(D_l^v\cos(\tilde{k}_v\Delta v) + D_l^w\cos(\tilde{k}_w\Delta w)\right)\sin\left(\frac{2l-1}{2}\tilde{k}_u\Delta u\right)\Bigg]^2, \end{aligned} \tag{6}$$

where $\tilde{\mathbf{k}} = \tilde{k}_u\hat{\mathbf{u}} + \tilde{k}_v\hat{\mathbf{v}} + \tilde{k}_w\hat{\mathbf{w}}$ is the numerical wavenumber.

[1] The notation $f|^{n}_{i_1,i_2,i_3}$ denotes the value of component f at point $(u,v,w) = (i_1\Delta u, i_2\Delta v, i_3\Delta w)$ and instant $t = n\Delta t$.

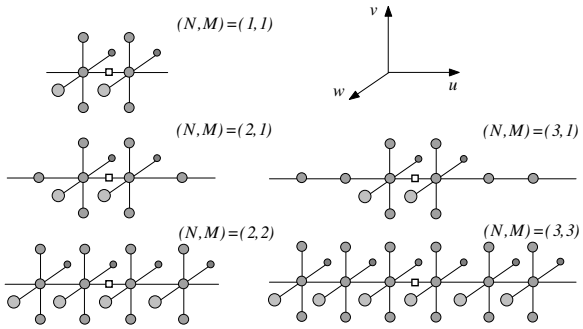

Fig. 1. Shape and size of the 3D spatial operators, for different choices of the parameters (N, M). The small square indicates the respective point of calculation.

The FDTD renditions that adopt operators (5) are conditionally stable, complying with the following upper bounds for the time-steps:

$$\Delta t \leqslant \left[c_0 \sqrt{\sum_{(u,v,w)} \frac{1}{\Delta u^2} \left(\sum_{l=1}^{N} (-1)^{l-1} C_l^u + 2 \sum_{l=1}^{M} (-1)^l (D_l^v + D_l^w) \right)^2} \right]^{-1}, \tag{7}$$

which are determined after performing the necessary von Neumann analysis. The stability limits for known schemes (e.g. Yee's algorithm, Fang's (2,4) method) can be derived from (7) as well.

Despite the fact that arbitrarily large values may be selected for parameters N, M (pursuing the highest level of accuracy), our research is confined to $N = 1, 2, 3$ and $M = 1, 2, 3$. These choices have been found to enable sufficient improvement over standard approaches, implying at the same time small or no aggravation of the entailed computational burden. In addition, maintaining the general structure of (2), (3) in the update equations contributes significantly in preserving much of the simplicity pertinent to the classic Yee scheme, which is deemed a feature of considerable importance.

3.2. Definition of error estimators

We now focus our attention to the design of operators (5) that guarantee low error levels. As known, it is impossible to find an analytical solution for (6), which would otherwise accommodate an error analysis. Instead, the evaluation of FDTD-related inaccuracies is attempted in an implicit – but equally reliable – manner. Although error formulae based on the dispersion relations could be theoretically developed (see, for instance, [18]), the procedure described below would be significantly more complex. Therefore, we choose to follow a slightly different path.

Let us assume plane waves propagating along a direction specified by the angles (θ, ϕ) in the spherical coordinate system. If $\hat{\mathbf{n}} = \sin\theta\cos\phi\hat{\mathbf{x}} + \sin\theta\sin\phi\hat{\mathbf{y}} + \cos\theta\hat{\mathbf{z}} = n_x\hat{\mathbf{x}} + n_y\hat{\mathbf{y}} + n_z\hat{\mathbf{z}}$ is the unit vector toward this direction and $\eta = \sqrt{\mu/\epsilon}$ the intrinsic impedance of the background medium, the electric-field intensity is related to the magnetic-field intensity through

$$\mathbf{E} = -\eta\hat{\mathbf{n}} \times \mathbf{H}. \tag{8}$$

The magnetic-field vector comprises three individual components,

$$\begin{bmatrix} H_x \\ H_y \\ H_z \end{bmatrix} = \begin{bmatrix} \sin\theta'\cos\phi' \\ \sin\theta'\sin\phi' \\ \cos\theta' \end{bmatrix} H, \tag{9}$$

where, apparently, (θ', ϕ') are characteristic of the field's polarization. Taking (8) and (9) into account, Maxwell's equation $\epsilon\partial_t\mathbf{E} = \nabla \times \mathbf{H}$ reduces to the following three scalar equations:

$$-\eta\epsilon\frac{\partial H}{\partial t}\begin{bmatrix} n_y\cos\theta' - n_z\sin\theta'\sin\phi' \\ n_z\sin\theta'\cos\phi' - n_x\cos\theta' \\ n_x\sin\theta'\sin\phi' - n_y\sin\theta'\cos\phi' \end{bmatrix} = \begin{bmatrix} 0 & -\frac{\partial H}{\partial z} & \frac{\partial H}{\partial y} \\ \frac{\partial H}{\partial z} & 0 & -\frac{\partial H}{\partial x} \\ -\frac{\partial H}{\partial y} & \frac{\partial H}{\partial x} & 0 \end{bmatrix}\begin{bmatrix} \sin\theta'\cos\phi' \\ \sin\theta'\sin\phi' \\ \cos\theta' \end{bmatrix}. \tag{10}$$

By substituting plane-wave forms $H = H_0 e^{\jmath(\omega t - \tilde{k}_x x - \tilde{k}_y y - \tilde{k}_z z)}$ $(\jmath = \sqrt{-1})$ in (10), and applying the proposed approximants, we are led to the compact formulation

$$[\mathcal{F}(\omega,\tilde{k},\theta,\phi)] = \begin{bmatrix} \mathcal{F}_y(\omega,\tilde{k},\theta,\phi)\cos\theta' - \mathcal{F}_z(\omega,\tilde{k},\theta,\phi)\sin\theta'\sin\phi' \\ \mathcal{F}_z(\omega,\tilde{k},\theta,\phi)\sin\theta'\cos\phi' - \mathcal{F}_x(\omega,\tilde{k},\theta,\phi)\cos\theta' \\ \mathcal{F}_x(\omega,\tilde{k},\theta,\phi)\sin\theta'\sin\phi' - \mathcal{F}_y(\omega,\tilde{k},\theta,\phi)\sin\theta'\cos\phi' \end{bmatrix} = [0], \tag{11}$$

where

$$\mathcal{F}_u(\omega,\tilde{k},\theta,\phi) = \frac{1}{c_0\Delta t}\sin\left(\frac{\omega\Delta t}{2}\right)n_u - \frac{1}{\Delta u}\sum_{l=1}^{N} C_l^u \sin\left(\frac{2l-1}{2}\tilde{k}_u\Delta u\right) - \frac{2}{\Delta u}\sum_{l=1}^{M}[D_l^v\cos(\tilde{k}_v\Delta v) + D_l^w \times \cos(\tilde{k}_w\Delta w)]\sin\left(\frac{2l-1}{2}\tilde{k}_u\Delta u\right). \tag{12}$$

In order to ensure algorithmic reliability, the constant coefficients C_l^u, D_l^v, D_l^w, that minimize the difference between the numerical $\tilde{k}$ and the exact wavenumber $k = \omega/c_0$ should be calculated. We assert that an equivalent approach is to enforce $\tilde{\mathbf{k}}(\omega,\theta,\phi) = \mathbf{k}(\omega)$ in (11) and require that the value of $[\mathcal{F}(\omega,k,\theta,\phi)]$ $(= [\mathcal{F}(\omega,\theta,\phi)])$ be as close to zero as possible. Apparently, $[\mathcal{F}(\omega,\theta,\phi)]$ cannot vanish for all frequencies/propagation angles, since this would imply a complete elimination of dispersion and anisotropy errors under any discretization conditions. However, one may intuitively realize that the closer the value of $[\mathcal{F}]$ is to zero, the more accurate the corresponding FDTD scheme will be. Consequently, it is a natural choice to use $[\mathcal{F}]$ as a measure of the inherent discretization inaccuracies and pursue the determination of the parametric operators via an error-minimization process. The latter apparently requires treating each $\mathcal{F}_u$, $u = x,y,z$, separately (the next subsection is concerned with this analysis). It is interesting to note that analogous formulas were proposed for the dispersion-relation-preserving schemes in [19] (although derived via different considerations, by assuming specific (TE_z) polarization for the numerical plane-wave solutions). The allegation that the individual $\mathcal{F}_u$ expressions constitute reliable descriptions of the inherent errors can be further supported, if their behavior is examined in case of algorithms with well-known properties. For instance, the validity of the following conclusions is easily certified (see Appendix A for details):

- In the case of Yee's method, we find that $\mathcal{F}_u^{\mathrm{Yee}}(\omega,\theta,\phi) = \mathrm{O}(\Delta u^2) + \mathrm{O}(\Delta t^2)$.
- For the (2,4) FDTD scheme, we obtain $\mathcal{F}_u^{(2,4)}(\omega,\theta,\phi) = \mathrm{O}(\Delta u^4) + \mathrm{O}(\Delta t^2)$.
- For Fang's fourth-order approach, it is proved that $\mathcal{F}_u^{(4,4)}(\omega,\theta,\phi)$ converges to zero at a fourth-order rate.

3.3. Analysis of error estimators

Before proceeding further, a crucial point is to recognize that, despite the dependence of $[\mathcal{F}]$ on three variables (ω,θ,ϕ), its minimization is actually required at *specific* frequencies and for *all* propagation angles. Optimization for some particular θ, ϕ will produce small errors along individual directions of propagation, a property that can be advantageous only in certain types of problems (involving e.g. guided wave propagation). Nevertheless, a globally useful numerical approach is generally expected to be capable of ensuring accurate field calculations irrespective of (θ,ϕ). On the other hand, a similar observation is not valid when the accuracy dependence on frequency is examined, as FDTD schemes are not necessary to be reliable for all possible wavenumbers coupled to the grid. Recall that wideband simulations refer to specific parts of the spectrum (known in advance), as these are mainly determined by the spectral content of the excitation sources. In addition, dispersion artifacts become more detrimental, if they correspond to coarser discretizations (hence, high-frequency regions pose the most severe accuracy requirements). Consequently, one is satisfied by a numerically

reliable solution only within specified frequency bands and, therefore, band-limited optimizations seem to be sufficient.

The aforementioned observations indicate that we should reformulate the error estimators in a suitable manner, in order to facilitate their minimization at selected frequencies, without overlooking the fact that the error mitigation should be performed irrespective of the direction of wave propagation. Keeping these matters in mind, let us initially consider the case of $\mathcal{F}_z$. The proposed design procedure is based on the expansion of $\mathcal{F}_z$ with respect to spherical surface harmonics [25], defined as

$$Y_n^m(\theta,\phi)=\sqrt{\frac{(2n+1)}{2(\delta_m+1)}\frac{(n-m)!}{(n+m)!}}P_n^m(\cos\theta)\cos(m\phi). \tag{13}$$

$P_n^m(\cos\theta)$ are associated Legendre polynomials, $n=0,1,2,\ldots,m=0,1,\ldots,n$, and

$$\delta_m=\begin{cases}1, & \text{if } m=0,\\ 0, & \text{if } m\neq 0.\end{cases} \tag{14}$$

$\mathcal{F}_z$ comprises terms of the form $\sin(\alpha\cos\theta)$, $\sin(\alpha\cos\theta)\cos(\beta\sin\theta\cos\phi)$ and $\sin(\alpha\cos\theta)\cos(\beta\sin\theta\sin\phi)$. Regarding the first one, it has been shown in [19] that its series expansion consists of harmonic functions with $m=0$:

$$\sin(\alpha\cos\theta)=\sum_{n=0}^{\infty}c_{2n+1}(\alpha)Y_{2n+1}^0(\theta,\phi), \tag{15}$$

where

$$c_n(\alpha)=\sqrt{(2n+1)\pi}\mathcal{T}_n(\alpha), \tag{16}$$

$$\mathcal{T}_n(\alpha)=\int_0^{\pi}\sin(\alpha\cos\theta)P_n(\cos\theta)\sin\theta\,\mathrm{d}\theta \tag{17}$$

and the integral $\mathcal{T}_n$ is obtained through the recursive formula

$$\mathcal{T}_n(\alpha)=\left[\frac{2(2n-3)}{2n-5}-\frac{(2n-1)(2n-3)}{\alpha^2}\right]\mathcal{T}_{n-2}(\alpha)-\frac{2n-1}{2n-5}\mathcal{T}_{n-4}(\alpha). \tag{18}$$

The necessary first two terms in (18) are given by

$$\mathcal{T}_1(\alpha)=\frac{2}{\alpha^2}(\sin\alpha-\alpha\cos\alpha), \tag{19}$$

$$\mathcal{T}_3(\alpha)=\frac{2}{\alpha^4}[(15-\alpha^2)\alpha\cos\alpha+3(2\alpha^2-5)\sin\alpha]. \tag{20}$$

Combining (15) with the addition theorem for Legendre polynomials [25] (which facilitates the change of the reference axis), we have been able to determine the expansion series for the remaining terms of $\mathcal{F}_z$. To accommodate the application of the addition theorem, the term $\sin(\alpha\cos\theta)\cos(\beta\sin\theta\cos\phi)$ is re-arranged according to the following form:

$$\sin(\alpha\cos\theta)\cos(\beta\sin\theta\cos\phi)=\frac{1}{2}\left[\sin\left(\sqrt{\alpha^2+\beta^2}\cos\gamma_1\right)+\sin\left(\sqrt{\alpha^2+\beta^2}\cos\gamma_2\right)\right]. \tag{21}$$

The angles γ_1 and γ_2 are the ones that the unit vector $\hat{\mathbf{n}}$ forms with the directions specified by $(\Theta_1,\Phi_1)=(\tan^{-1}(\beta/\alpha),0)$ and $(\Theta_2,\Phi_2)=(\tan^{-1}(\beta/\alpha),\pi)$ (as implied, Θ_i and Φ_i, $i=1,2$ are calculated with respect to the z- and x-axis, respectively). Taking (15) into account, the two terms in the right-hand side of (21) can be replaced by the equivalent formulas

$$\sin\left(\sqrt{\alpha^2+\beta^2}\cos\gamma_i\right)=\sum_{n=0}^{\infty}c_{2n+1}\left(\sqrt{\alpha^2+\beta^2}\right)Y_{2n+1}^0(\gamma_i,\phi) \tag{22}$$

for $i=1,2$. It is now easy to show that the implementation of the addition theorem results in

$$P_n(\cos\gamma_i) = P_n(\cos\Theta_i)P_n(\cos\theta) + 2\sum_{m=1}^{n}\frac{(n-m)!}{(n+m)!}P_n^m(\cos\Theta_i)P_n^m(\cos\theta)\cos[m(\phi-\Phi_i)]. \tag{23}$$

In essence, it is deduced that

$$\sin(\alpha\cos\theta)\cos(\beta\sin\theta\cos\phi) = \sum_{n=0}^{\infty}\sum_{m=0}^{n} c'_{2n+1,2m}(\alpha,\beta)Y_{2n+1}^{2m}(\theta,\phi), \tag{24}$$

which means that the examined term involves additional surface harmonics, compared to $\sin(\alpha\cos\theta)$. The analytic expression for the expansion coefficients is

$$c'_{n,m}(\alpha,\beta) = \sqrt{\frac{2^{1-\delta_m}(n-m)!}{(n+m)!}}P_n^m(\cos\theta_0)c_n(\gamma), \tag{25}$$

where

$$\theta_0 = \tan^{-1}\left(\frac{\beta}{\alpha}\right), \tag{26}$$

$$\gamma = \sqrt{\alpha^2+\beta^2}. \tag{27}$$

The analysis of $\sin(\alpha\cos\theta)\cos(\beta\sin\theta\sin\phi)$ is similar to (24), with the only difference being the sign of individual terms. In fact, we have

$$\sin(\alpha\cos\theta)\cos(\beta\sin\theta\sin\phi) = \sum_{n=0}^{\infty}\sum_{m=0}^{n} c''_{2n+1,2m}(\alpha,\beta)Y_{2n+1}^{2m}(\theta,\phi), \tag{28}$$

where the multiplying coefficients are related to those of (25) via

$$c''_{n,m}(\alpha,\beta) = (-1)^{m/2}c'_{n,m}(\alpha,\beta). \tag{29}$$

Taking into account all the aforementioned findings, the expansion of $\mathcal{F}_z$ is given by

$$\mathcal{F}_z(\omega,\theta,\phi) = \sum_{n=0}^{\infty}\sum_{m=0}^{n} C_{2n+1,2m}^{z}(\omega)Y_{2n+1}^{2m}(\theta,\phi), \tag{30}$$

where

$$C_{n,m}^{z}(\omega) = \sqrt{\frac{4\pi}{3}}\frac{1}{c_0\Delta t}\sin\left(\frac{\omega\Delta t}{2}\right)\delta_{n-1}\delta_m - \frac{1}{\Delta z}\sum_{l=1}^{N} C_l^z c_n\left(\frac{2l-1}{2}k\Delta z\right)\delta_m$$
$$-\frac{2}{\Delta z}\sum_{l=1}^{M}\left[D_l^x c'_{n,m}\left(\frac{2l-1}{2}k\Delta z, k\Delta x\right) + D_l^y c''_{n,m}\left(\frac{2l-1}{2}k\Delta z, k\Delta y\right)\right]. \tag{31}$$

As seen, the first dominant terms in the expansion series are related to the functions Y_1^0, Y_3^0, Y_3^2, Y_5^0, Y_5^2, Y_5^4, etc.

Before proceeding further, it should be mentioned that the above results, although derived for the $\mathcal{F}_z$ estimator (which corresponds to the z-derivative), are sufficient for the other two error expressions as well. Specifically, no additional analysis for $\mathcal{F}_x$ or $\mathcal{F}_y$ is necessary, as long as the harmonic functions in their expansion series are expressed with respect to their corresponding axis (x-axis for $\mathcal{F}_x$, y-axis for $\mathcal{F}_y$) and not the z-axis (this is equivalent to performing a simple axis rotation before the calculation of each series). Under this assumption, the remaining expansions are easily obtained from (30) by circularly permuting the position of the spatial increments.

4. Novel FDTD schemes with optimized performance

In this section, the presented mathematical analysis is exploited for the determination of the parametric finite-difference operators, so as to comply with specified accuracy requirements. Obviously, the natural choice

is to select those values for the constants (C_l^u, D_l^v, D_l^w) that guarantee low levels for the proposed error estimators. As one may suspect, the series expansion of the latter facilitates this task, since the vanishing of the dominant terms should suffice to guarantee small values for $[\mathcal{F}]$. It is also understood that the accomplishment of this objective at a given frequency ω implies the zeroing of the corresponding multiplying coefficients $\mathcal{C}_{n,m}^u(\omega)$ which, among others, are linear functions of the unknowns (due to the "decoupling" (30) of the spectral and angular dependence, the selection of a "preferred" direction of propagation is avoided). Consequently, our initial quest for algorithmic reliability leads to a set of algebraic equations, whose solution defines operators satisfying the imposed accuracy restrictions. Clearly, the maximum number of vanishing terms is directly related to the number of unknowns, which depends on the stencil size of the spatial approximations. Therefore, our methodology unveils the inevitable connection between the entailed computational overhead and the maximum attainable accuracy, which, as shown later, cannot be reached by conventional FDTD formulations.

In the following paragraphs, a family of FDTD algorithms with different capabilities is presented. To render them easily identifiable, we will be using the notation $S\{N, M, L\}$, where the parameters N, M describe the shape and size of the spatial stencil (recall (5)), while L indicates the number of design frequency points (this parameter is further explained later and can be set equal to either 1 or 2).

4.1. Narrowband optimization

Maximizing the accuracy within a small frequency band probably constitutes the simplest case, because it requires error minimization at only one frequency point, designated by the part of the spectrum we are interested in. This approach is deemed appropriate when most or all of the electromagnetic power related to a numerical simulation is confined within a narrow area, around an angular frequency ω_0. It is apparent that the minimization of $\mathcal{F}_u$ at ω_0 should be sufficient to ensure an adequate algorithmic performance. Taking into account that each of the spatial operators incorporates $N + 2M$ undetermined coefficients, we seek an equal number of algebraic equations. In other words, the single-frequency tuning of the discretization scheme requires the vanishing of $N + 2M$ terms in each of the error estimators. For instance, the $S\{1,1,1\}$ scheme adopts a z-derivative approximation that is determined from the solution of the three equations $\mathcal{C}_{1,0}^z(\omega_0) = \mathcal{C}_{3,0}^z(\omega_0) = \mathcal{C}_{3,2}^z(\omega_0) = 0$, or the system

$$\begin{bmatrix} c_1\left(\frac{k_0\Delta z}{2}\right) & 2c'_{1,0}\left(\frac{k_0\Delta z}{2}, k_0\Delta x\right) & 2c''_{1,0}\left(\frac{k_0\Delta z}{2}, k_0\Delta y\right) \\ c_3\left(\frac{k_0\Delta z}{2}\right) & 2c'_{3,0}\left(\frac{k_0\Delta z}{2}, k_0\Delta x\right) & 2c''_{3,0}\left(\frac{k_0\Delta z}{2}, k_0\Delta y\right) \\ 0 & 2c'_{3,2}\left(\frac{k_0\Delta z}{2}, k_0\Delta x\right) & 2c''_{3,2}\left(\frac{k_0\Delta z}{2}, k_0\Delta y\right) \end{bmatrix} \begin{bmatrix} C_1^z \\ D_1^x \\ D_1^y \end{bmatrix} = \begin{bmatrix} \sqrt{\frac{4\pi}{3}}\frac{\Delta z}{c_0\Delta t}\sin\left(\frac{\omega_0\Delta t}{2}\right) \\ 0 \\ 0 \end{bmatrix}, \tag{32}$$

where $k_0 = \omega_0/c_0$. Similar systems are formulated for the other two spatial approximations. As expected, the same procedure is applied for the extraction of the $S\{2,1,1\}$, $S\{2,2,1\}$ and $S\{3,3,1\}$ algorithms, through the solution of 4×4, 6×6 and 9×9 systems, respectively. For reference, the coefficients that define the operators of the $S\{N, M, 1\}$ methods, optimized at 10 cells per wavelength, are given in Table 1.

To gain a better insight into the individual properties of each scheme, the overall discretization error at four design frequencies is estimated in Table 2. In order to take into account all possible directions of propagation, inaccuracies related to the numerical phase velocity $\tilde{c}(\omega, \theta, \phi)$ are evaluated via the definition

Table 1
Coefficients for $S\{N, M, 1\}$ schemes, optimized for a $\lambda/10$ grid density

	$S\{1,1,1\}$	$S\{2,1,1\}$	$S\{2,2,1\}$	$S\{3,3,1\}$
C_1^u	0.8394744	0.9045670	1.0680281	1.1427505
C_2^u	0.0	−0.0099276	−0.0238882	−0.0523487
C_3^u	0.0	0.0	0.0	0.0020441
$D_1^{v,w}$	0.0429073	0.0331249	0.0144771	0.0071881
$D_2^{v,w}$	0.0	0.0	−0.0049752	−0.0036786
$D_3^{v,w}$	0.0	0.0	0.0	0.0007709

Table 2
Error e_{3D} vs cell size for various schemes when $\Delta x = 1.5\Delta y = 2\Delta z$

Scheme	$\Delta x = \lambda/10$	$\Delta x = \lambda/20$	$\Delta x = \lambda/40$	$\Delta x = \lambda/80$	Rate
Yee	3.357×10^{-3}	8.295×10^{-4}	2.068×10^{-4}	5.166×10^{-5}	~2.01
(4,4)	9.416×10^{-5}	5.928×10^{-6}	3.713×10^{-7}	2.322×10^{-8}	~4.00
$S\{1,1,1\}$	5.837×10^{-6}	3.591×10^{-7}	2.232×10^{-8}	1.839×10^{-9}	~3.88
$S\{2,1,1\}$	3.787×10^{-6}	2.321×10^{-7}	1.443×10^{-8}	9.010×10^{-10}	~4.01
$S\{2,2,1\}$	6.836×10^{-8}	1.049×10^{-9}	1.632×10^{-11}	2.665×10^{-13}	~5.99
$S\{3,3,1\}$	1.347×10^{-9}	5.115×10^{-12}	2.084×10^{-14}	2.804×10^{-16}	~7.40

$$e_{3D}(\omega) = \frac{1}{4\pi}\int_0^{\pi}\int_0^{2\pi}\left|1-\frac{\tilde{c}(\omega,\theta,\phi)}{c_0}\right|\sin\theta\,\mathrm{d}\theta\,\mathrm{d}\phi. \tag{33}$$

For each case, the maximum allowable time-step is considered. From the presented results, it can be deduced that both the $S\{1,1,1\}$ and $S\{2,1,1\}$ schemes accomplish fourth-order convergence at the design points, with the second technique ensuring extra improvement of approximately 35%. On the other hand, the $S\{2,2,1\}$ method exhibits a sixth-order rate of convergence, while the $S\{3,3,1\}$ version is capable of improving its accuracy at an eighth-order rate (apparently, the slightly lower average rate given in Table 2 is due to the fact that machine precision is rapidly reached). For comparison purposes, the results concerning Yee's scheme, as well as Fang's (4,4) method, are also calculated, verifying the superior quality of the proposed algorithms.

At this point, it should be clarified that the proposed optimization procedure does not produce valid results for all possible combinations of N and M. In essence, the requirements imposed when enforcing very low values for the error estimators cannot be always satisfied by all types of difference approximations (such a difficulty was not encountered in the two-dimensional case [26], at least for the examined examples). This fact undoubtedly exposes the inherent complexity of any effort aiming at the improvement of FDTD performance in 3D configurations. Nevertheless, the schemes developed in this paper are deemed sufficient for the vast majority (if not all) of contemporary electromagnetic problems.

4.2. Broadband optimization

Presumably, the proposed $S\{N,M,1\}$ algorithms are not designed to handle simulations with wideband spectral content. A more appropriate way to control discretization artifacts over an extended frequency range is to require the minimization of the error expressions at two distinct frequency points (as, in this way, one expects weaker dispersion effects within the spectrum's part defined by these points). If the latter are denoted by ω_1 and ω_2 ($\omega_1 > \omega_2$), the necessary equations can be extracted from the vanishing of the first p terms of $\mathcal{F}_u(\omega_1,\theta,\phi)$ and the first $N+2M-p$ terms of $\mathcal{F}_u(\omega_2,\theta,\phi)$, $1 \leqslant p \leqslant N+2M-1$. Complying with this strategy, we have been able to derive the following $S\{N,M,2\}$ schemes (the conditions pertaining to the error-control process are also given):

- $S\{2,1,2\}$ scheme: $\mathcal{C}^u_{1,0}(\omega_1) = \mathcal{C}^u_{3,0}(\omega_1) = \mathcal{C}^u_{3,2}(\omega_1) = \mathcal{C}^u_{1,0}(\omega_2) = 0$.
- $S\{2,2,2\}$ scheme: $\mathcal{C}^u_{1,0}(\omega_1) = \mathcal{C}^u_{3,0}(\omega_1) = \mathcal{C}^u_{3,2}(\omega_1) = \mathcal{C}^u_{5,0}(\omega_1) = \mathcal{C}^u_{5,2}(\omega_1) = \mathcal{C}^u_{1,0}(\omega_2) = 0$.
- $S\{3,1,2\}$a scheme: $\mathcal{C}^u_{1,0}(\omega_1) = \mathcal{C}^u_{3,0}(\omega_1) = \mathcal{C}^u_{3,2}(\omega_1) = \mathcal{C}^u_{5,0}(\omega_1) = \mathcal{C}^u_{1,0}(\omega_2) = 0$.
- $S\{3,1,2\}$b scheme: $\mathcal{C}^u_{1,0}(\omega_1) = \mathcal{C}^u_{3,0}(\omega_1) = \mathcal{C}^u_{3,2}(\omega_1) = \mathcal{C}^u_{1,0}(\omega_2) = \mathcal{C}^u_{3,0}(\omega_2) = 0$.

Table 3
Coefficients for $S\{N,M,2\}$ schemes, optimized for frequencies corresponding to $\lambda/10$ and $\lambda/30$ grid densities

	$S\{2,1,2\}$	$S\{2,2,2\}$	$S\{3,1,2\}$a	$S\{3,1,2\}$b
C^u_1	1.0309707	0.9968470	1.0744774	1.0840809
C^u_2	−0.0291920	−0.0178172	−0.0463203	−0.0505004
C^u_3	0.0	0.0	0.0032697	0.0041123
$D^{v,w}_1$	0.0141467	0.0225807	0.0120345	0.0119717
$D^{v,w}_2$	0.0	−0.0028121	0.0	0.0

We have essentially pursued the elimination of a larger number of terms at the higher frequency ω_1, in order to mitigate errors emanating from coarse spatial resolutions. For reference, the values of the operators' coefficients are given in Table 3, when it is selected $\omega_1/\omega_2 = 3$ for the design frequencies and $\Delta x = \Delta y = \Delta z = \lambda_1/10$. Furthermore, Figs. 2–4 illustrate the spectral response of the proposed wideband techniques for various

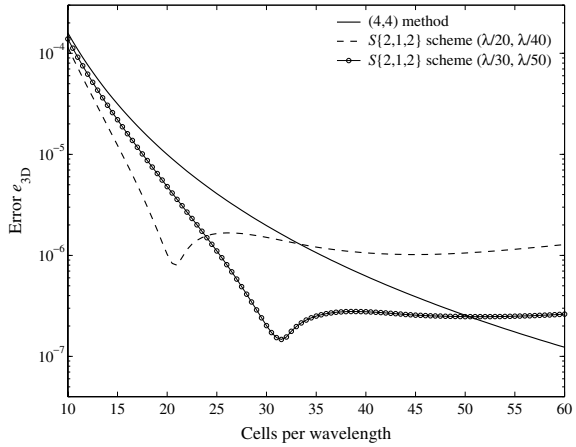

Fig. 2. Error e_{3D} versus mesh density for the $S\{2,1,2\}$ scheme, optimized at (20, 40) and (30, 50) cells per wavelength.

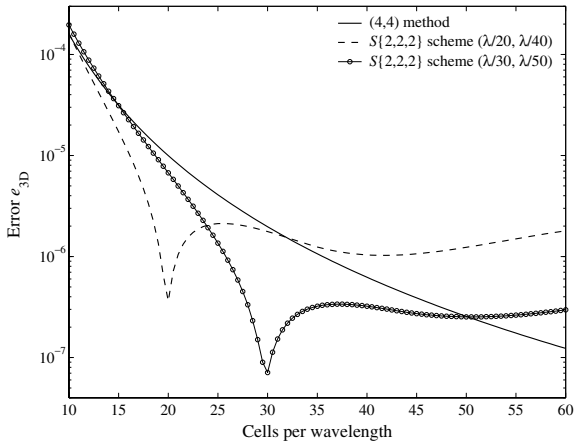

Fig. 3. Error e_{3D} versus mesh density for the $S\{2,2,2\}$ scheme, optimized at (20, 40) and (30, 50) cells per wavelength.

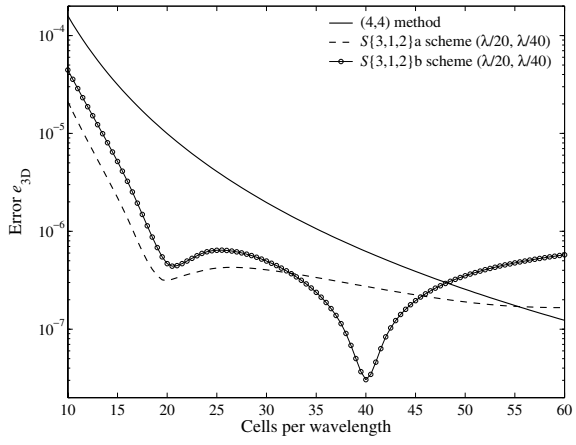

Fig. 4. Error e_{3D} versus mesh density for the $S\{3,1,2\}$a and $S\{3,1,2\}$b schemes, optimized at 20 and 40 cells per wavelength.

pairs of optimization frequencies. As seen, the $S\{2,1,2\}$ scheme presents an acute minimum at ω_1, and at the same time outperforms the (4,4) method at all higher frequencies. A similar behavior is observed in the case of the $S\{2,1,2\}$ scheme, which also accomplishes slightly more intense changes in the error curves. On the other hand, the $S\{3,1,2\}$a rendition is characterized by a mildly fluctuating error level within a wide frequency range, whereas the $S\{3,1,2\}$b technique exhibits two distinct error minima. These figures definitely manifest the attractive characteristics, as well as the upgraded performance of the new broadband algorithms. The upcoming numerical tests will also validate these theoretical findings.

5. Discussion on boundary operators

A problem commonly encountered in the application of high-order FDTD methods is concerned with the proper interface/boundary treatment, when modeling media with different electromagnetic properties. In essence, difficulties emerge form the extended stencil of the adopted difference operators, whose implementation becomes problematic in areas within the vicinity of material boundaries. Since a naive or oversimplified interface modeling can severely degrade the overall performance of the utilized high-order algorithm (thus cancelling any possible merits), the solution of this issue has been the subject of investigation in various papers. We hereafter mention some representative efforts.

For instance, a simple solution was applied in [14], where the high-order spatial operators were replaced by second-order ones in positions near the interfaces. Unfortunately, such an approach, although straightforward and easy to implement, may seriously affect both the accuracy and stability of the interior scheme. A similar, but more sophisticated solution, was developed in [27], which was based on the hybridization of the (2,4) FDTD method with a second-order subgridding strategy. Alternatively, other authors have proposed the substitution of the extended operators with one-sided counterparts in the critical areas, so that operator stencils never cross boundaries. This concept was efficiently utilized in [4,9], while one-sided formulas were also referenced in [13], together with proper high-order extrapolation schemes. Furthermore, [6] combined analogous expressions with low-pass spatial filters, in order to suppress spurious high-frequency components that can potentially lead to numerical instabilities. According to a different perspective, the concept of directly enforcing the physical jump conditions on the discrete level was extensively investigated in [28], where methodologies based on a derivative-matching procedure and utilizing additional fictitious nodes were presented. Another practice was investigated in a recent publication [29], which dictates local or global regularization of the discontinuous permittivity functions for mesh-conforming configurations. Consequently, as the aforementioned methodologies are characterized by diverse advantages/diasdvantages, computational complexity and flexibility, the issue of high-order interface modeling in FDTD methodologies remains an open matter requiring further investigation.

6. Numerical results

The first numerical example is concerned with the time evolution of the field that corresponds to two distinct modes, appearing in a cavity with perfectly conducting boundaries (the configuration is cubic with 10-cm sides). The modes are characterized by the indices (3,2,2) and (0,1,4) and, consequently, resonate at the same frequency, equal to 6.181 GHz. The desired waveforms are excited by enforcing the exact field distributions at the first time-step. A total of 20^3m cells, $m = 1,2,4$, are used to construct the lattice, while the duration of the corresponding simulations is selected $5000m\Delta t_{\mathrm{Yee}}$ s (Δt_{Yee} is the time-step limit for the Yee scheme). Fig. 5 illustrates the maximum $L_2(t)$ errors with respect to E_x, observed during the refinement process. The upgraded reliability, along with high rates of convergence (which are in agreement with the previous theoretical analysis), are evident for the optimized FDTD methods.

To better appreciate the practical gains of the proposed algorithms, the maximum errors in the aforementioned problem are plotted in Fig. 6 as a function of the required simulation times (all tests were performed on a single workstation with a Pentium 4-3.8 GHz processor and 1 GB of memory). It can be seen that the optimized schemes provide a very attractive tradeoff between attained accuracy and necessary computational cost, as they are all proven to be more efficient than Fang's fourth-order method. Clearly, the enhanced error levels of the new operators sufficiently compensate for their slightly increased computational complexity, thus estab-

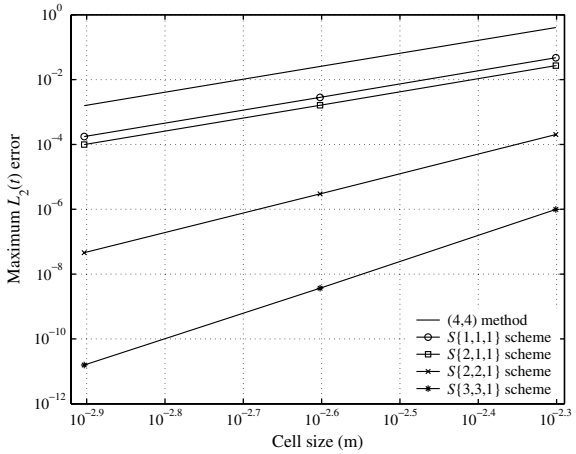

Fig. 5. Maximum values of the L_2 error versus the cell size, in the simulation of two cavity-modes with the same resonant frequency.

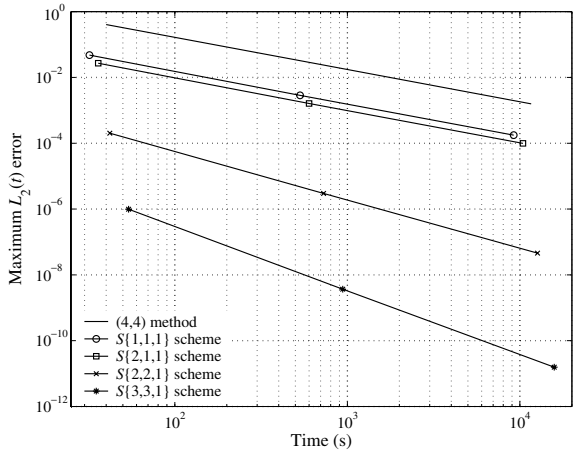

Fig. 6. Maximum values of the L_2 error versus the total simulation time, in the simulation of two cavity-modes with the same resonant frequency.

lishing reliable computational models. In fact, compared to the conventional (4,4) approach, the qualitative superiority of the $S\{2,2,1\}$ and $S\{3,3,1\}$ schemes becomes even more emphasized in refined grids, due to their better convergence features.

Next, we consider the case of a 14.3-cm-long rectangular waveguide with a 2.286×1.016 cm cross-section. Specifically, the propagation of the TE_{11} mode is simulated, by assigning boundary values to the two ports according to the exact field distribution at all time-steps. Considering that the cutoff frequency is 16.145 GHz, the excitation frequency is set equal to 19 GHz. The structure is discretized with $14m \times 6m \times 89m$ grids, $m = 1, 2, 4$, and each simulation is carried out for $5000m\Delta t_{\mathrm{Yee}}$ s. The maximum values of the calculated $L_2(t)$ errors for each case are shown in Fig. 7, where the superiority of the $S\{N, M, 1\}$ schemes in time-harmonic situations is once again verified. Similarly to the previous example, the proposed FDTD methods exhibit the behavior revealed theoretically, thus enabling the advantageous and highly efficient exploitation of computational resources.

The performance of the optimized algorithms is also evaluated on the basis of the involved computational cost in the waveguide problem. For this reason, we set as our objective the error value that is produced by the (4,4) method, when the $28 \times 12 \times 178$ grid is used ($\simeq 5.721 \times 10^{-2}$), for a time period of 15.82 ns (this corresponds to $10{,}000\Delta t_{\mathrm{Yee}}$ for this grid resolution). Given the desired level of accuracy, the minimum grid densities

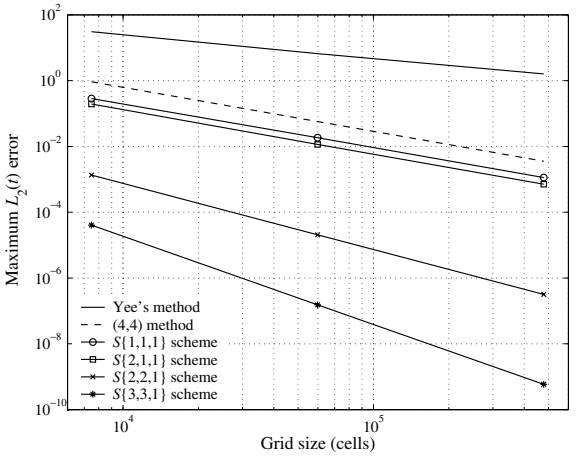

Fig. 7. Maximum values of the L_2 error versus the computational domain's size (in cells), for the rectangular waveguide simulation.

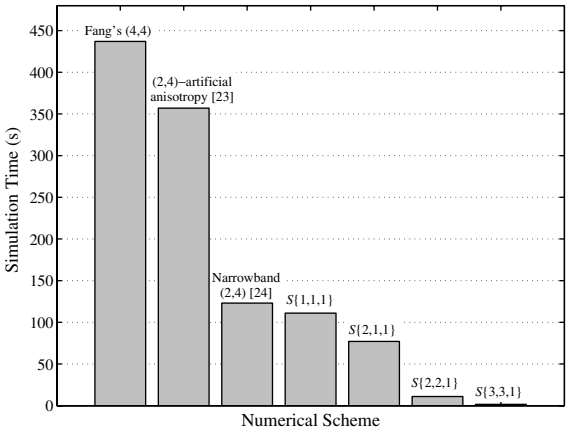

Fig. 8. Total simulation times of various FDTD schemes in the waveguide problem, for lattices ensuring a specific error threshold.

required to satisfy this threshold, as well as the respective simulation times, are determined for all schemes. In addition, we consider the performance of two other reduced-dispersion techniques, proposed in the past: the (2,4) method incorporating artificially anisotropic materials [23], and a narrowband technique, which encompasses modified spatial and temporal expressions in a (2,4) computational stencil [24]. The obtained results are exhibited in Fig. 8 and the significant reduction of the computational burden is evident, in the cases of the optimized schemes. For reference, the grid sizes for each algorithm are given: $25 \times 11 \times 156$ for the method of [23], $21 \times 9 \times 131$ for the narrowband (2,4) method, $21 \times 9 \times 134$ for the $S\{1,1,1\}$ scheme, $19 \times 8 \times 119$ for the $S\{2,1,1\}$ technique, $11 \times 5 \times 66$ for the $S\{2,2,1\}$ approach and only $6 \times 3 \times 37$ for the $S\{3,3,1\}$ algorithm. Clearly, the proposed solutions permit the utilization of coarser lattices to reach a desired error level, ensuring considerable savings in terms of both computer time and memory.

The potential of the optimized methodologies in long-term examination of electromagnetic interactions is demonstrated in the next numerical experiment, where a $10 \times 14 \times 18$ cm cavity is modeled. Three modes are excited, identified by the indices (1,1,1), (1,4,2) and (3,3,5). Since their resonant frequencies are 2.022, 4.834 and 6.919 GHz, respectively, the $S\{N,M,2\}$ algorithms are implemented, within a computational domain discretized by a $28 \times 39 \times 50$ cell lattice. From Fig. 9, where the error in E_z at a specific position is drawn, the significantly lower rate of increase can be verified for the $S\{2,1,2\}$ (5.6 GHz, 3 GHz) and $S\{3,1,2\}$b (6 GHz, 3 GHz) techniques, when compared to the (4,4) method (the design frequencies are shown in paren-

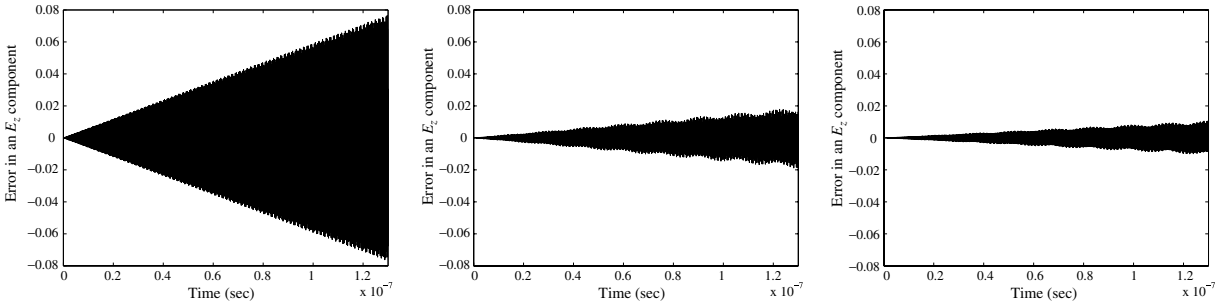

Fig. 9. Time evolution of the error in the E_z component, produced by the (4,4) (left), $S\{2,1,2\}$ (middle) and $S\{3,1,2\}$b (right) methods, in the case of a cavity under multimodal excitation.

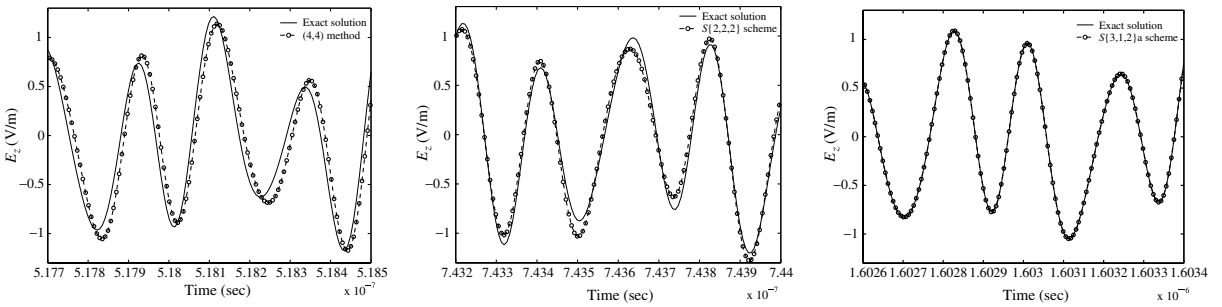

Fig. 10. Predicted waveforms by the (4,4) (left), $S\{2,2,2\}$ (middle) and $S\{3,1,2\}$a (right) methods, for the problem of a cavity under multimodal excitation.

Table 4
Required mesh size and overall simulation's duration for a given error level and various schemes, in the multimodal cavity problem

Method	L_2 error	Grid size (cells)	Simulation time (s)	Speedup
Fang's (4,4)	1.022×10^{-3}	$48 \times 66 \times 85$	3449	–
$S\{2,2,2\}$	9.471×10^{-4}	$43 \times 60 \times 77$	2199	1.6
$S\{2,1,2\}$	9.351×10^{-4}	$34 \times 47 \times 60$	830	4.2
$S\{3,1,2\}$b	9.578×10^{-4}	$28 \times 39 \times 50$	443	7.8
$S\{3,1,2\}$a	9.981×10^{-4}	$23 \times 32 \times 41$	190	18.2

theses). If the maximum values of the $L_2(t)$ error are compared, an improvement by 14 and 27.6 times is found, respectively, thus revealing the quality of the practical merits. Furthermore, Fig. 10 presents a comparison between calculated and exact waveforms, after several thousands of iterations have been completed. Even in the case of Fang's fourth-order approach, the predicted field values are characterized by non-trivial phase errors (after approximately $75{,}000\Delta t_{(4,4)}$ s), whereas milder discrepancies are detected for the $S\{2,2,2\}$ algorithm after $107{,}650\Delta t_{(4,4)}$ s. An even more reliable field prediction is provided by the $S\{3,1,2\}$a technique, where no deviation from the exact solution can be physically observed after a period of $232{,}000\Delta t_{(4,4)}$.

Considering the previously analyzed configuration, we examine the computational burden produced by each numerical scheme, in order to satisfy a pre-determined error level. Specifically, it is required that an L_2 norm value (with respect to E_x) close to 10^{-3} be ensured, after a simulated time period of approximately 34.53 ns. Under these assumptions, the necessary grid size and corresponding simulation times are given in Table 4, along with the extracted speedup factors, with respect to Fang's (4,4) method. These results clearly demonstrate the advantages of utilizing properly optimized finite-difference schemes, as they are capable of guaranteeing considerable computational savings for a given accuracy level. It is easily understood that, despite their increased cost per node, the coarser spatial lattices permit the selection of larger time steps,

resulting in faster simulations (up to 18 times in this example). To make a last comment, given that the design frequencies were selected rather empirically, other choices may lead to even better performance.

7. Conclusions

The aim of this paper has been the development of highly reliable FDTD techniques for the numerical solution of the time-dependent Maxwell's equations on 3D Cartesian lattices. This goal has been fulfilled by proposing novel differencing schemes, which avoid the shortcomings induced by conventional design approaches. By initially specifying merely the structure of the spatial operators, new algorithms are founded on the minimization of proper algebraic expressions that serve as reliable error indicators. In essence, algorithmic performance is fully adapted to fundamental features of both the examined problem (e.g. spectral content) and the corresponding discrete model (e.g. space–time discretization density). As proved, the most prominent quality of the developed approaches is their optimized character, not only at time-harmonic situations, but at extended frequency bands as well, thus permitting highly efficient – yet uncomplicated – treatment of contemporary, 3D electromagnetic problems, possibly subject to strict accuracy requirements. In this way, efficient exploitation of computational resources is ensured and powerful electromagnetic models are constructed.

Appendix A

We herein examine the convergence characteristics of the proposed error estimators, when adapted to well-known FDTD schemes. Specifically, the corresponding $\mathcal{F}_u$ expressions are analyzed according to Taylor series expansion and we investigate whether (or not) the anticipated behavior is exhibited, in order to further justify the validity of their designation as reliable error indicators.

Case 1: Yee's method. For the case of Yee's algorithm, we have $C_1^u = 1$, $C_l^u = 0$ for $l \neq 1$, $D_l^v = D_l^w = 0$. By using these values, it is obtained

$$\mathcal{F}_u^{\mathrm{Yee}}(\omega,\theta,\phi) = \frac{1}{48}k_u^3\Delta u^2 - \frac{\omega^2}{48}k_u\Delta t^2 + \mathrm{O}(\Delta u^4) + \mathrm{O}(\Delta t^4), \tag{A.1}$$

which is characteristic of second-order schemes.

Case 2: (2,4) method. For Fang's (2,4) technique, it is $C_1^u = 9/8$, $C_2^u = -1/24$, $C_3^u = 0$, $D_l^v = D_l^w = 0$. The Taylor expansion of the error estimator now yields

$$\mathcal{F}_u^{(2,4)}(\omega,\theta,\phi) = \frac{3}{1280}k_u^5\Delta u^4 - \frac{\omega^2}{48}k_u\Delta t^2 + \mathrm{O}(\Delta u^6) + \mathrm{O}(\Delta t^4), \tag{A.2}$$

which reveals, once again, the true convergence rate of the examined technique.

Case 3: (4,4) method. Fang's (4,4) FDTD scheme adopts a fourth-order leapfrog integrator and incorporates update equations with the form of (2), (3). The latter can be considered to apply spatial operators similar to (5), as long as we set $C_1^u = \frac{9}{8} - \frac{1}{24}(c_0\Delta t)^2(\frac{3}{\Delta u^2} + \frac{2}{\Delta v^2} + \frac{2}{\Delta w^2})$, $C_2^u = -\frac{1}{24} + \frac{1}{24\Delta u^2}(c_0\Delta t)^2$, $D_1^v = \frac{1}{24\Delta v^2}(c_0\Delta t)^2$, $D_1^w = \frac{1}{24\Delta w^2}(c_0\Delta t)^2$, $C_3^u = D_2^v = D_2^w = D_3^v = D_3^w = 0$. Under these conditions, we find that

$$\begin{aligned}\mathcal{F}_u^{(4,4)}(\omega,\theta,\phi) = {} & \frac{\omega^4}{3840}k_u\Delta t^4 + \frac{3}{1280}k_u^5\Delta u^4 - \frac{1}{1152}k_u[c_0^2\Delta t^2(k_u^2(3k_u^2 + k_v^2 + k_w^2)\Delta u^2 + 2k_v^4\Delta v^2 \\ & + 2k_w^4\Delta w^2)] + \mathrm{O}(\Delta u^6) + \mathrm{O}(\Delta t^6) + \text{mixed terms of 6th order}\end{aligned} \tag{A.3}$$

i.e. the error estimator converges to zero at a fourth-order rate.

References

[1] K.S. Yee, Numerical solution of initial boundary value problems involving Maxwell's equations in isotropic media, IEEE Trans. Antennas Propagat. 14 (1966) 302–307.

[2] A. Taflove, S.C. Hagness, Computational Electrodynamics: The Finite-Difference Time-Domain Method, Norwood, Artech House, Boston, London, 2000.

[3] J. Fang, Time domain computation for Maxwell's equations, Ph.D. dissertation, Univ. California, Berkeley, 1989.

[4] A. Yefet, P.G. Petropoulos, A staggered fourth-order accurate explicit finite difference scheme for the time-domain Maxwell's equations, J. Comput. Phys. 168 (2001) 286–315.
[5] J.L. Young, D. Gaitonde, J.J.S. Shang, Toward the construction of a fourth-order difference scheme for transient EM wave simulation: staggered grid approach, IEEE Trans. Antennas Propagat. 45 (1997) 1573–1580.
[6] J.S. Shang, High-order compact-difference schemes for time-dependent Maxwell equations, J. Comput. Phys. 153 (1999) 312–333.
[7] E. Turkel, A. Yefet, On the construction of a high order difference scheme for complex domains in a Cartesian grid, Appl. Numer. Math. 33 (2000) 113–124.
[8] H. Spachmann, R. Schuhmann, T. Weiland, Higher order time integration schemes for Maxwell's equations, Int. J. Numer. Modelling: Electron. Networks Dev. Fields 15 (2002) 419–437.
[9] Z. Xie, C.-H. Chan, B. Zhang, An explicit fourth-order orthogonal curvilinear staggered-grid FDTD method for Maxwell's equations, J. Comput. Phys. 175 (2002) 739–763.
[10] Z. Shao, Z. Shen, Q. He, G. Wei, A generalized high order finite-difference time-domain method and its application in guided-wave problems, IEEE Trans. Microwave Theory Tech. 51 (2003) 856–861.
[11] S.K. Lele, Compact finite difference schemes with spectral-like resolution, J. Comput. Phys. 103 (1992) 16–42.
[12] C.K.W. Tam, J.C. Webb, Dispersion-relation-preserving finite difference schemes for computational acoustics, J. Comput. Phys. 107 (1993) 262–281.
[13] D.W. Zingg, H. Lomax, H. Jurgens, High-accuracy finite-difference schemes for linear wave propagation, SIAM J. Sci. Comput. 17 (1996) 328–346.
[14] M.F. Hadi, M. Piket-May, A modified FDTD (2,4) scheme for modeling electrically large structures with high-phase accuracy, IEEE Trans. Antennas Propagat. 45 (1997) 254–264.
[15] I. Tsukerman, A class of difference schemes with flexible local approximation, J. Comput. Phys. 211 (2005) 659–699.
[16] J.B. Cole, A high-accuracy realization of the Yee algorithm using non-standard finite differences, IEEE Trans. Microwave Theory Tech. 45 (1997) 991–996.
[17] T. Kashiwa, H. Kudo, Y. Sendo, T. Ohtani, Y. Kanai, The phase velocity error and stability condition of the three-dimensional nonstandard FDTD method, IEEE Trans. Magn. 38 (2002) 661–664.
[18] S. Wang, F.L. Teixeira, A three-dimensional angle-optimized finite-difference time-domain algorithm, IEEE Trans. Microwave Theory Tech. 51 (2003) 811–817.
[19] S. Wang, F.L. Teixeira, Dispersion-relation-preserving FDTD algorithms for large-scale three-dimensional problems, IEEE Trans. Antennas Propagat. 51 (2003) 1818–1828.
[20] G. Sun, C.W. Trueman, Optimized finite-difference time-domain methods based on the (2,4) stencil, IEEE Trans. Microwave Theory Tech. 53 (2005) 832–842.
[21] B. Finkelstein, R. Kastner, Finite difference time domain dispersion reduction schemes, J. Comput. Phys. 221 (2007) 422–438.
[22] J.W. Nehrbass, J.O. Jevtić, R. Lee, Reducing the phase error for finite-difference methods without increasing the order, IEEE Trans. Antennas Propagat. 46 (1998) 1194–1201.
[23] T.T. Zygiridis, T.D. Tsiboukis, A dispersion-reduction scheme for the higher order (2,4) FDTD method, IEEE Trans. Magn. 40 (2004) 1464–1467.
[24] T.T. Zygiridis, T.D. Tsiboukis, Low-dispersion algorithms based on the higher-order (2,4) FDTD method, IEEE Trans. Microwave Theory Tech. 52 (2004) 1321–1327.
[25] J.A. Stratton, Electromagnetic Theory, McGraw-Hill Book Company, New York and London, 1941.
[26] T.T. Zygiridis, T.D. Tsiboukis, Design of optimized FDTD schemes for the accurate solution of EM problems, IEEE Trans. Magn. 42 (2006) 811–814.
[27] S.V. Georgakopoulos, R.A. Renaut, C.A. Balanis, C.R. Birtcher, A hybrid fourth-order FDTD utilizing a second-order FDTD subgrid, IEEE Microwave Wireless Comp. Lett. 11 (2001) 462–464.
[28] S. Zhao, G.W. Wei, High-order FDTD methods via derivative matching for Maxwell's equations with material interfaces, J. Comput. Phys. 200 (2004) 60–103.
[29] E. Kashdan, E. Turkel, High-order accurate modeling of electromagnetic wave propagation across media – grid conforming bodies, J. Comput. Phys. 218 (2006) 816–835.